JOM, Vol. 64, No. 2, 2012
DOI: 10.1007/s11837-012-0241-4

Processing of Advanced Cast Alloys for A-USC Steam Turbine Applications

PAUL D. JABLONSKI,[1,3] JEFFERY A. HAWK,[1]
CHRISTOPHER J. COWEN,[1] and PHILIP J. MAZIASZ[2]

1.—National Energy Technology Laboratory, Albany, OR, USA
e-mail: paul.jablonski@netl.doe.gov . 2.—Oak Ridge National Laboratory, Oak Ridge, TN, USA.
3.—e-mail: paul.jablonski@netl.doe.gov

The high-temperature components within conventional supercritical coal-fired power plants are manufactured from ferritic/martensitic steels. To reduce greenhouse-gas emissions, the efficiency of pulverized coal steam power plants must be increased to as high a temperature and pressure as feasible. The proposed steam temperature in the DOE/NETL Advanced Ultra Supercritical power plant is high enough (760°C) that ferritic/martensitic steels will not work for the majority of high-temperature components in the turbine or for pipes and tubes in the boiler due to temperature limitations of this class of materials. Thus, Ni-based superalloys are being considered for many of these components. Off-the-shelf forged nickel alloys have shown good promise at these temperatures, but further improvements can be made through experimentation within the nominal chemistry range as well as through thermomechanical processing and subsequent heat treatment. However, cast nickel-based superalloys, which possess high strength, creep resistance, and weldability, are typically not available, particularly those with good ductility and toughness that are weldable in thick sections. To address those issues related to thick casting for turbine casings, for example, cast analogs of selected wrought nickel-based superalloys such as alloy 263, Haynes 282, and Nimonic 105 have been produced. Alloy design criteria, melt processing experiences, and heat treatment are discussed with respect to the as-processed and heat-treated microstructures and selected mechanical properties. The discussion concludes with the prospects for full-scale development of a thick section casting for a steam turbine valve chest or rotor casing.

INTRODUCTION

Conventional supercritical coal-fired power plants utilize steam turbines and generators to produce electricity and typically operate at efficiencies on the order of 35% to 37%.[1] Operation at higher temperatures and pressures can lead to greater efficiencies, resulting in both reduced fuel consumption and lower greenhouse-gas emissions.[2] The goals of the US Department of Energy's Advanced Power Systems Initiatives include Advanced Ultra Supercritical (A-USC) power generation from coal which requires steam conditions of up to 760°C and 35 MPa.[3] Such systems have the ability to reach efficiencies on the order of 47%. Higher efficiency will translate to reduced CO_2 production for the same amount of energy produced, thereby facilitating a reduction in greenhouse-gas emissions, or if combined with oxy-combustion and carbon capture and sequestration (CCS) technologies, an easy-to-manipulate CO_2 stream will be produced that will facilitate capture and sequestration. The terms subcritical, supercritical (SC), ultrasupercritical (USC), and A-USC for coal power plants are roughly defined for the steam as follows: subcritical at below 22 MPa and 375°C, SC at above 22.1 MPa and between 538°C and 565°C, USC at above 565°C, and A-USC at temperatures above about 700°C with pressures reaching 35 MPa. Austenitic alloys, both steel and nickel-base, generally possess sufficient creep strength to work at 700°C. However, austenitic alloys present other difficulties such as low

(Published online February 11, 2012)

thermal conductivity and high thermal expansion coefficients. Nickel-base superalloys must be used above 675°C.[1] Suitable nickel base superalloys are required in A-USC conditions that exist in both the boiler and the turbine to meet high-temperature creep strength requirements in these pressurized systems.[3]

Nickel-base alloys are quite complex with chemistry, processing, and heat treatment critically important and interdependent in achieving long-term microstructural stability and strength. The chemistry and crystal structure of the matrix (FCC γ) plus the strengthening precipitates (either γ' or γ'' or both) make processing nickel-base alloys in the large sizes needed for steam turbine rotor shafts or gas turbine disk and spacer segments difficult. In addition, if composite rotors are envisioned to reduce base material costs, thermal expansion mismatch, dissimilar alloy welding (e.g., precipitate-strengthened nickel-base alloys to solution-strengthened nickel-base alloys and/or ferritic or martensitic steels) and subsequent heat treatment make the problem especially difficult. Also, many of the nickel-based alloys identified for use as steam turbine components were initially developed for aero-engine applications or oil and gas conditions where high strength and creep resistance for only several thousand hours were needed. In steam turbine rotating components, creep lifetimes greater than 100,000 h are required. In addition, the alloys must have adequate uniaxial strength and good toughness, that is, for example, high yield strength to withstand the stresses within the rotor upon start-up and shut down. Also important are the fatigue capability of the alloy, specifically, low cycle fatigue resistance as well as thermal fatigue and hold-time fatigue resistance for the rotor segments as well as other thick section components such as the casing, and high cycle fatigue capability for the airfoils. Identifying alloys that possess the requisite combination of creep strength, yield strength, and fatigue capability is difficult, especially in steam. One benefit of utilizing nickel-base alloys is their good overall general hot corrosion and oxidation resistance.

Evaluation of current materials for A-USC steam turbine casings shows that only age-hardenable γ'-strengthened nickel-base alloys have the strength required for the desired application temperature using current steam turbine design practice. These alloys, by necessity, have significant amounts of aluminum, which forms this major matrix strengthening precipitate in the FCC γ matrix. The production of these alloys involves combinations of highly controlled casting processes such as electroslag remelting (ESR), vacuum induction melting (VIM), or vacuum arc remelting (VAR). Production of large steam turbine casings requires the use of air casting processes. When cast in air, the aluminum in the nickel alloys oxidizes, leading to aluminum loss from the melt. This has the potential to cause porosity or to introduce inclusions, with subsequent reduction in the amount of γ' and possibly resulting in significant decreases in mechanical strength. Improved air-based casting processes or new alloy formulations without (or minimizing) aluminum additions are needed to realize large volume, thick section castings with requisite strength for A-USC steam turbine casings.

Consider, for example, the high-pressure (HP) rotor. The rotor is one of the most critical elements in the steam turbine. From a design requirement, a creep rupture strength of at least ~100 MPa at 100,000 h is necessary at the operational temperature as a minimum life requirement. Ideally, creep rupture strength of ~100 MPa at 250,000 h would be better, as this is the usual expected life of a conventional USC steam turbine.

The following mechanical minimum requirements define a rough guide for the wrought nickel alloys in the steam turbine including the rotor, airfoils, bolts, valve internals, etc. The creep potential of the wrought nickel-base alloys must possess at least 100 MPa rupture strength at 760°C for 100,000 h. A minimum 0.2% yield strength greater than 400 MPa in the radial direction (or transverse for bar stock) at 760°C is required for highly stressed regions, although higher strength would be desirable. Toughness >55 MPa$\cdot\sqrt{m}$ provides good fracture toughness at room temperature for these alloys.

For those sections of the turbine where cast product forms are used, other requirements must be met, some mechanically related such as those for the wrought nickel alloys while others have to do with manufacturing operations. From a mechanical performance point of view, having adequate tensile yield strength is very important, both at room temperature for start up and also at the use temperature. Room-temperature yield strength greater than 550 MPa is required, depending on the steam turbine design, while at 760°C the yield strength must be greater than 350 MPa, again subject to the specific original equipment manufacturer turbine design requirements. Creep strength is the same as for wrought nickel superalloy, that is, ~100 MPa at 760°C for at least 100,000 h.

From a manufacturing perspective, being able to cast nickel superalloy in large sections from 100 mm to 200 mm thick and at high yields of >5000 kg is important, as is being able to weld onto the casting. If the casting is welded in some manner, either to a pipe or to adjacent sections of a much larger casing or as part of a casing repair process, then a post-weld heat treatment will be required. Consequently, having as simple a heat treatment as possible for the cast nickel component would be desirable. Of course, cost is important as well, but in this case manufacturing expense would be dependent upon the expense of the raw materials used in the cast article, any intellectual property associated with the casting process or alloy composition, availability of organizations capable of casting such large articles (i.e., having competing organizations would be

desirable), welding processes associated with casing production and repair, ease and duration of heat treatment of the cast article, etc.

The nickel alloys that are available today as castings generally fall into two categories. The first category is solid solution-strengthened alloys, which tend to be weldable, even in thick sections. Unfortunately, these alloys suffer from loss of strength at high temperature relative to their γ' strengthened analogs. The second category are the γ' formers, which possess high strength, particularly at high γ' volume fractions of $>50\%$, but these tend to have limited ductility and are not weldable in thick sections. Examples of the solution-strengthened alloys include IN625, IN909, and Haynes 230, which are wrought alloys also available as castings. Examples of γ' forming cast alloys include IN100, Mar-M247, and IN939, which are high-strength casting alloys with limited ductility and are not weldable in thick sections. It should be noted that these alloys are not available as wrought products due to the high γ' volume fraction and inherent limited ductility, leading to a lack of formability even in the hot condition. Additionally, since these alloys typically contain several wt.% Al, they are usually vacuum cast to avoid oxidation of the Al. The steam turbine casing weighs several tons, and section thickness is on the order of 100 mm or more, making vacuum casting impractical. In general, wrought alloys have superior weldability in comparison with high-γ' casting alloys due to their reduced Al and Ti content and sluggish γ' precipitation kinetics attributable to a higher Ti/Al ratio. Thus, traditionally wrought alloys with moderate γ' volume fraction have potential to meet both casting process and mechanical property goals.

The objective of this work is to screen air casting, heat treatment, and resulting mechanical properties of promising wrought superalloys. The alloys being considered in this research are available as wrought products such as plate or bar. While nominal alloy chemistry was employed, close attention was made to minor alloy additions with respect to alloy castability and mechanical performance while remaining within the alloy specification.

EXPERIMENTAL PROCEDURES

Alloy Design and Manufacture

Computational thermodynamic modeling tools (Thermo-Calc)[4] were first used to model the alloy phase contents of the nominal alloy chemistry. Following this, the impact of varying each of the specified elements was considered by use of a vertical section through the alloy phase diagram. Finally, the tendency for each alloy to segregate during nonequilibrium solidification was evaluated with the use of the Scheil module within Thermo-Calc. Once an alloy formulation was set, the remelt materials were gathered from stocks of high-purity raw materials. Each 6800 g heat was melted under 200 mTorr of Ar in an induction furnace. The melt was cast with 50°C superheat above the Thermo-Calc predicted liquidus for each alloy. The melts were poured into 100-mm-diameter round graphite molds, which also incorporated a zirconia wash coat to prevent pickup of additional carbon. The molds were submerged in loose sand to help slow the cooling rate and better emulate the slow cooling conditions of a full-size casing component (Fig. 1). After casting, a 2-mm-thick diametrical slice was removed from each ingot top for chemical analysis. The transition element chemistries were determined by wavelength-dispersive x-ray florescence using a Rigaku ZSX Primus II and utilizing NIST-traceable standards, and reported values are accurate to 0.01 wt.%. Carbon chemistries were determined with a LECO CS444LS using NIST-certified standards, and reported values are accurate to 0.002 wt.%. The ingots were subsequently bisected diametrically, and one half was metallographically prepared for macrograin etching. Subsequently, the secondary dendrite arm spacing was determined in the columnar and central equiaxed zones. Following this, the ingot halves were instrumented and wired together for a computationally optimized multistep homogenization heat treatment.[5,6] The homogenization step results in better dispersal of the alloy constituents, reducing segregation and improving mechanical performance. The homogenized alloys were subsequently peak aged in the following fashion: (1) N105 was heated to between 1050°C and 1065°C for 16 h and then air cooled (AC), followed by subsequent aging at 850°C for 16 h and then AC; (2) alloy 263: 880°C/8 h/AC; and (3) H282: 1050°C/2 h/AC + 1010°C/2 h/AC + 788°C/8 h/AC.

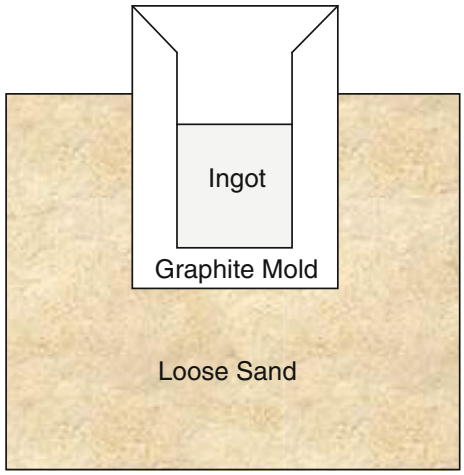

Fig. 1. Schematic representation showing the experimental casting layout consisting of a graphite mold immersed in loose sand such that the cast ingot top surface was below the level of the sand. Additional details are found within the text.

Alloy Fluidity Studies

A Taylor fluidity spiral mold[7] was used to determine the relative fluidity of alloy 263 and H282. Master heats of these two alloys were made in a similar manner to those heats discussed above, except that the melts were poured into steel tubes in order to produce remelt stock. This step was crucial since the base alloy constituents have little oxidation resistance in comparison with the alloy. The alloy stock was remelted in air and cast into fluidity spiral molds made from sodium silicate bonded sand. The pour temperature and travel distance of each heat were measured and recorded.

Mechanical Properties

The peak age heat-treated ingots were cut into 10-mm slab shapes which were subsequently cut into tensile bar blanks. The tensile bar blanks were machined into cylindrical geometry tensile specimens, which employed $L = 4D$ geometry. Tensile and creep testing were performed in accordance with ASTM E-21 and E-139 at 800°C with instrumented data acquisition.

Microstructural Evaluation

Creep-tested samples were sectioned parallel to the loading axis, ground to about mid-plane, before polishing via conventional metallographic procedures. The cross-sections were examined by scanning electron microscopy (SEM) using a combination of secondary-electron (SE) and backscatter-electron (BSE) imaging to evaluate the phases present.

RESULTS AND DISCUSSION

Alloy Design

Plots of predicted stable phases versus temperature for each of the alloys are shown in Figs. 2–4. Among these three alloys, N105 has the greatest amount of γ' (40%) at 760°C, followed by H282 (18%). Alloy 263 shows η as the majority strengthening phase at 760°C to 800°C rather than γ' (Fig. 4). It should be noted that, while μ is predicted in all the alloys, it was not observed in any of the alloys, and it is likely that its formation is kinetically limited. Likewise, η was predicted but not observed in alloy 263. The phase stability of alloy 263 was reconsidered with η suspended (Fig. 5). This new calculation showed about 10% γ' in alloy 263 at 760°C. Thus, the three alloys are predicted to contain differing amounts of the same phases in the neighborhood of 760°C to 800°C: γ', $M_{23}C_6$, and the balance being γ matrix. At 800°C, the predicted equilibrium contents of γ' in N105, Alloy 263, and H282 are 36.4 wt.%, 8.1 wt.%, and 16.7 wt.%, respectively.

The majority of the alloying elements were set to the mid-spec values (Table I). The exception to this

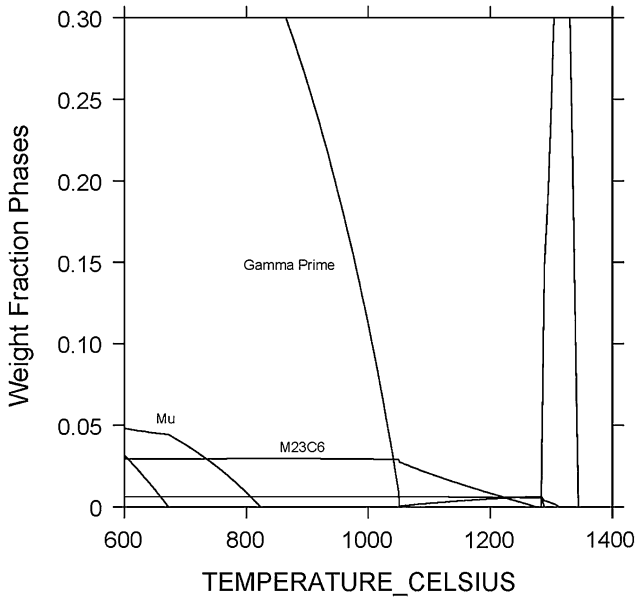

Fig. 2. Weight fraction of phases versus temperature for Nimonic 105 alloy.

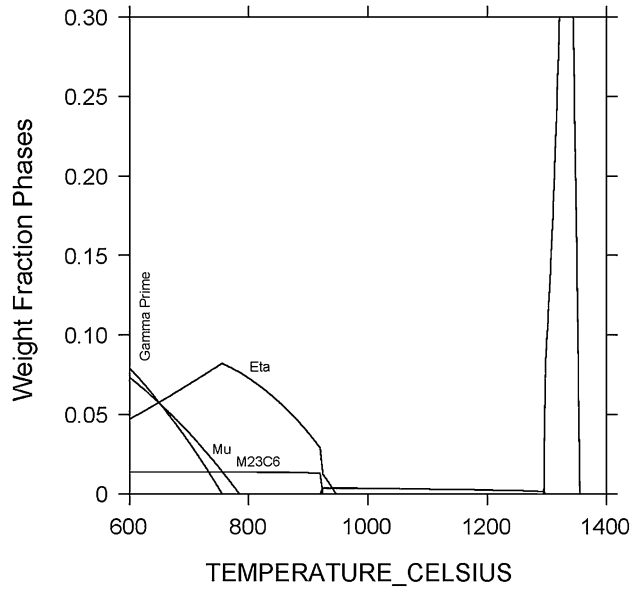

Fig. 3. Weight fraction of phases versus temperature for alloy 263.

rationale was the oxygen-active elements Al, Ti, C, Mn, and Si. The first two elements (i.e., Al and Ti) were set to a slightly lower value to reduce their potential to form oxides during melting. The remaining three elements (i.e., C, Mn, and Si) were set to a slightly higher level within nominal alloy specification limits to aid in protecting the melt from oxidation. Previous research has shown that maintaining Mn above 0.15 wt.% was critical for minimizing the loss of Cr in a 17-4PH steel during long-term air melt holds.[8] The lowest Mn level in this group of alloys was 0.24 wt.%, so these alloys met this criterion.

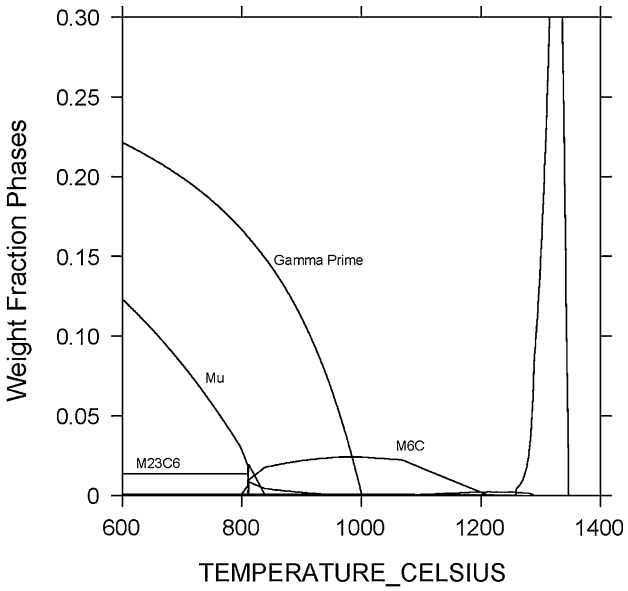

Fig. 4. Weight fraction of phases versus temperature for Haynes 282 alloy.

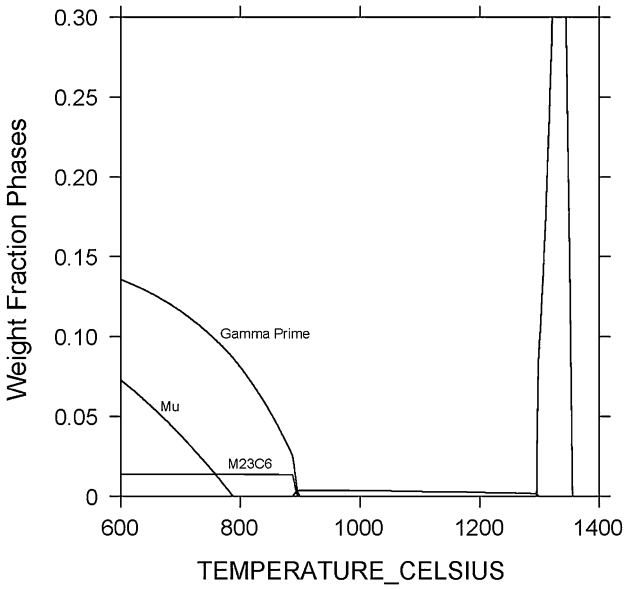

Fig. 5. Weight fraction of phases versus temperature for alloy 263, calculated with the η phase suspended.

The equilibrium and nonequilibrium solidification ranges for each alloy are summarized in Table II. The equilibrium solidification ranges were less than 100°C, and there was little difference between the values calculated for the "lean" chemistries versus those with high solute content for each of the alloys. The solidification range of the experimental chemistry (i.e., what was ultimately melted) fell between these two values. The nonequilibrium Scheil determined solidification ranges for each alloy was significantly greater than the equilibrium range (~200°C). However, there was generally little difference between the "lean" and high-solute nonequilibrium solidification ranges. Nimonic 105 was the exception to this trend, likely due to the relatively large allowable ranges of C, Mn, and Si, which tended to partition to the liquid and depress the incipient melt point. Thus, the formulations of each of the alloys were a balance between phase stability and impact upon solidification range and segregation.

Macrostructure

The macrograin structure of the ingots is revealed in Fig. 6. In general, the ingots contained a band of columnar grains emanating radially from the sidewall and upwards from the ingot bottom surface. The columnar grains were approximately one-fourth to one-third the length of the ingot radius. Inward of this columnar zone was found an equiaxed grain region. This overall grain structure is similar to the structure expected in a large sand casting of this geometry. The secondary dendrite arm spacing was measured to be 46 μm to 65 μm in the columnar zone and 82 μm to 92 μm in the equiaxed zone. No microporosity was observed beyond the large shrink cavity and adjacent mushy region.

Homogenization Heat Treatment

A homogenization heat treatment was developed[5,6] based on the Scheil–Gulliver[9,10] predicted segregation for each alloy as provided by the Scheil module in Thermo-Calc.[4] This profile was scaled to the measured microstructural features of the castings. The segregation profile was "homogenized" within the computer using the multicomponent diffusion program DICTRA.[11] The initial heat treatment temperature was adjusted to be safely below the incipient melt temperature for all the alloys based on the Scheil–Gulliver prediction. After preselected times at this lower temperature, the new incipient melt temperature was determined and the heat treatment conditions were adjusted accordingly. Figure 7 shows examples of the as-cast and homogenized microstructures of one of the alloys (N105). The inhomogeneity of the cast structure is clearly visible in the micrograph and is exhibited by very dark dendrite cores and light etching interdendritic regions. After homogenization the microstructure is very uniformly etched, indicating that the homogenization treatment was successful.

Fluidity

The results of the fluidity study are shown in Fig. 8. In general, the fluidity distance (i.e., the distance the molten metal flowed at a given temperature) increased monotonically with temperature above the liquidus. Although the data are limited, they suggest two linear regions above the liquidus: (1) a region from 0°C to ~175°C and (2) a region above ~175°C. The fluidity results of these

Table I. Experimental alloy chemistry of each heat, with the chemistry range for each alloy (in wt.% except as noted)

Alloy	Ni	Cr	Co	Mo	Ti	Al	Fe	Mn	Si	C	B (ppm)
N105	Bal	14.0–15.7	18.0–22.0	4.5–5.5	0.9–1.5	4.5–4.9		1.0*	1.0*	0.17*	30–100
Alloy 263	Bal	19.0–21.0	19.0–21.0	5.6–6.1	1.9–2.4	0.30–0.60	0.7*	0.6*	0.4*	0.04–0.08	
H282	Bal	18.5–20.5	9–11	8–9	1.9–2.3	1.38–1.65	1.5*	0.3*	0.15*	0.04–0.08	30–50
Experimental alloys											
N105	Bal	14.61	20.04	5.02	1.10	4.43		051	0.51	0.16	500
Alloy 263	Bal	19.68	19.98	5.74	2.04	0.40		0.50	0.34	0.07	
H282	Bal	19.22	9.84	8.48	2.08	1.44		0.24	0.15	0.07	100

*Maximum value.

Table II. Liquidus, solidus, equilibrium (eq) and nonequilibrium solidification temperatures, and ranges for the three alloys with nominal, minimum, and maximum alloy constituents

Alloy	Liquidus (°C)	Eq. Solidus (°C)	Noneq. Solidus (°C)	Eq. ΔT (°C)	Noneq. ΔT (°C)
N105	1346	1282	1130	64	216
Experimental					
Min	1378	1312	1219	66	159
Max	1312	1252	1084	60	228
Alloy 263	1365	1296	1139	69	226
Experimental					
Min	1372	1319	1180	53	192
Max	1345	1285	1130	60	215
H282	1347	1259	1164	88	183
Experimental					
Min	1359	1265	1175	94	184
Max	1336	1253	1155	83	181

For calculation purposes, the experimental chemistry was the same as what was cast; the "max" and "min" chemistries are found in Table I.

two alloys compare favorably with those of steels (i.e., as good as or better),[7,12] supporting the casting capability of these alloys. Also, while not tested explicitly with this mold configuration, no hot tears were observed on any of these spiral castings.

Mechanical Properties

Tensile behavior of the cast, homogenized, and aged alloys was similar to that of equivalent wrought products; for example, Fig. 9 shows the ultimate tensile strength (UTS) and yield strength (YS) behavior of wrought N105 from room temperature to 816°C. At isolated test temperatures there was some scatter in the UTS values of about 70 MPa to 125 MPa, while tests at the majority of the temperatures had scatter less than 25 MPa. Scatter in YS was less at between 20 MPa and 50 MPa. The interesting result of the cast alloy performance, although limited to one temperature, is the close correspondence in UTS at 800°C (similar to the 816°C values for UTS) and the very good agreement of YS at 800°C with those of the wrought N105.

Table III provides a summary of selected 0.2% YS and elongation data for wrought N105, alloy 263, and H282. Also included in the table are selected values for the cast materials. The wrought alloys were solutionized and then peak aged according to standard practice. The cast analogs were homogenized and then peak aged according to standard practice. It is interesting to note that the N105 alloy in the cast form behaved very similarly to the wrought alloy in terms of strength and ductility. For alloy 263 and H282, the cast versions were less strong and showed some decrease in ductility.

The cast alloy creep results are compared with the typical wrought alloy performance in Fig. 10. The overall results of the three alloys fell in order of γ' content, with N105 having the best creep performance followed closely by H282. For all three alloys, it was found that the cast versions performed comparably to their wrought counterparts. This is due in part to the homogenization heat treatment[5,6] given to each alloy prior to peak aging. Without this heat treatment, critical strengthening elements such as Al, Ti, and Mo would be

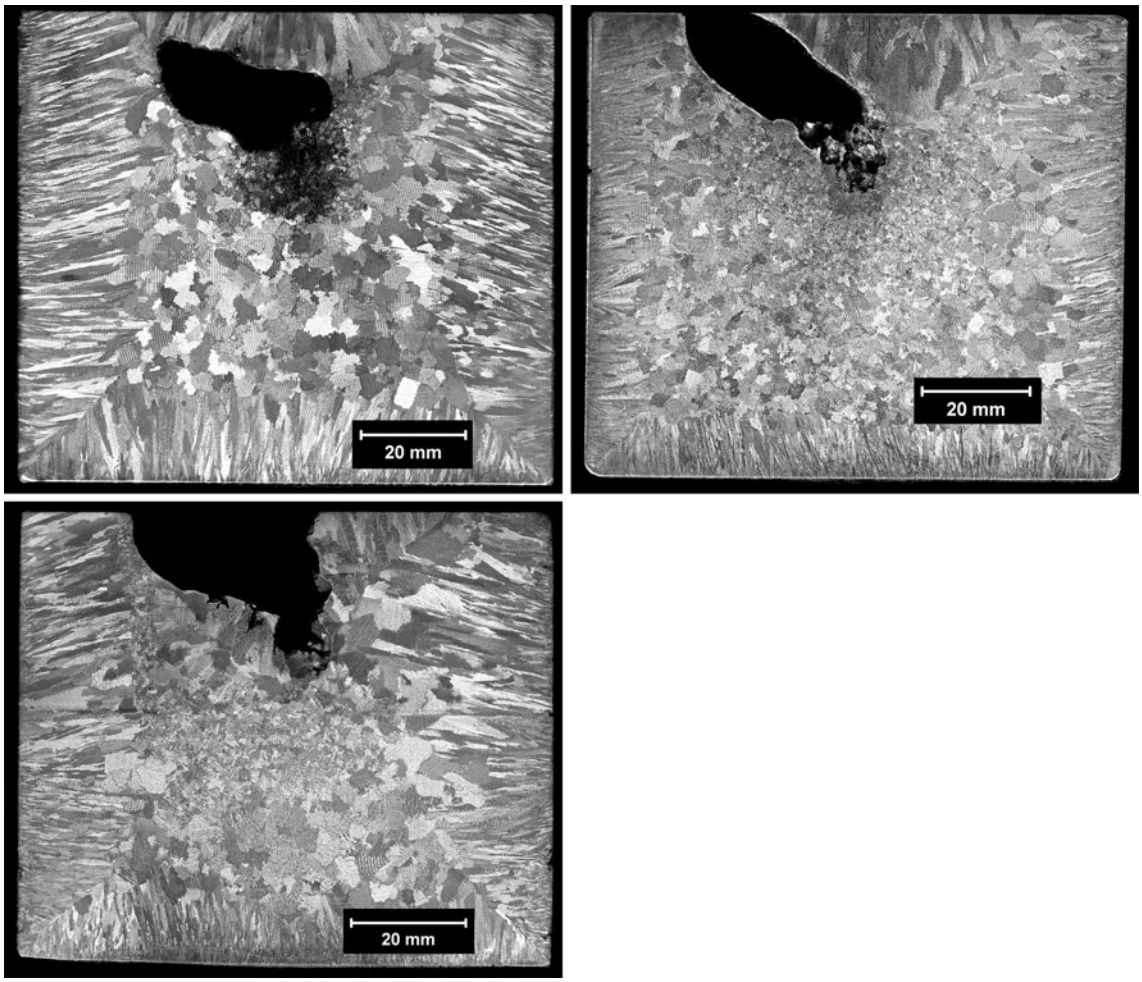

Fig. 6. Macrograin structures of the as-cast ingots (N105, upper left; alloy 263, upper right; H282, lower left). Note that approximately 2 mm to 3 mm had been removed from the ingot tops in a prior operation. Each ingot measures approximately 100 mm in diameter and consists of an outer columnar region surrounding an inner equiaxed zone with upper shrink cavity.

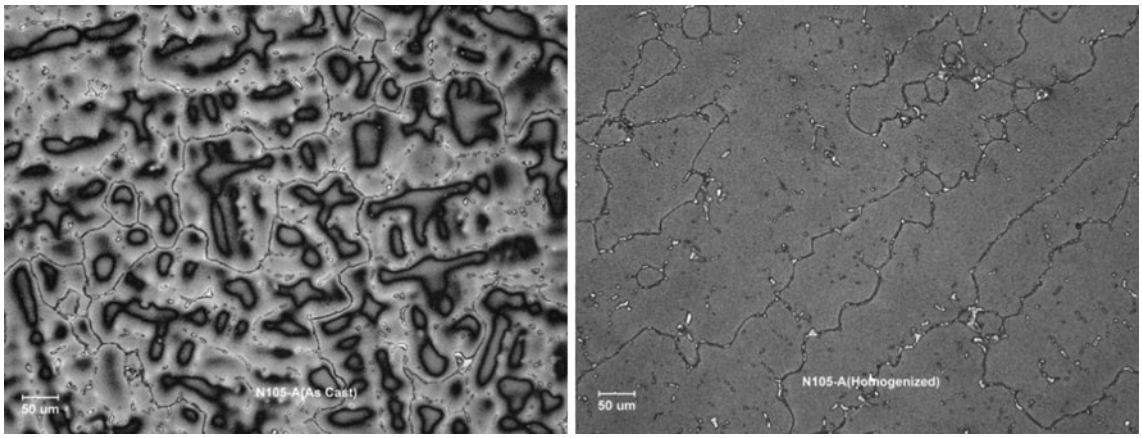

Fig. 7. The nonhomogenized as-cast microstructure with regions of dendritic segregation is shown on the left for N105. An equivalent region of microstructure after homogenization is shown on the right.

concentrated either in the dendrite cores or in the interdendritic regions of the cast material. This cast structure is refined in wrought alloys during ingot preheat and subsequent hot working operations. Of course, another feature of the cast microstructure favoring creep performance is the

large grain size (typically 100 μm to 300 μm in the equiaxed zone) compared with the wrought alloys (typically 20 μm to 100 μm).

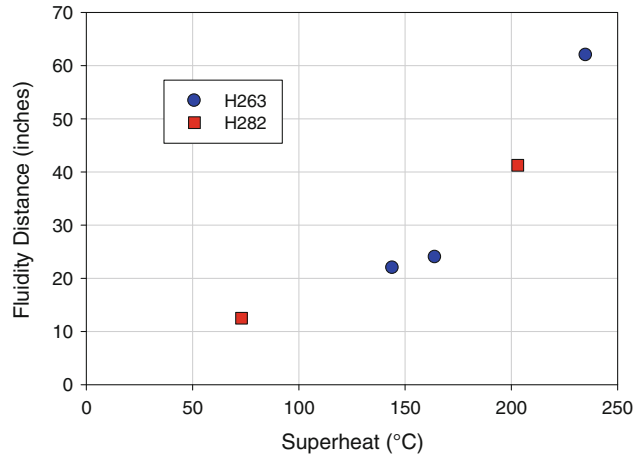

Fig. 8. Results of the fluidity spiral casting study, plotted as fluidity distance versus superheat for both alloy 263 and H282.

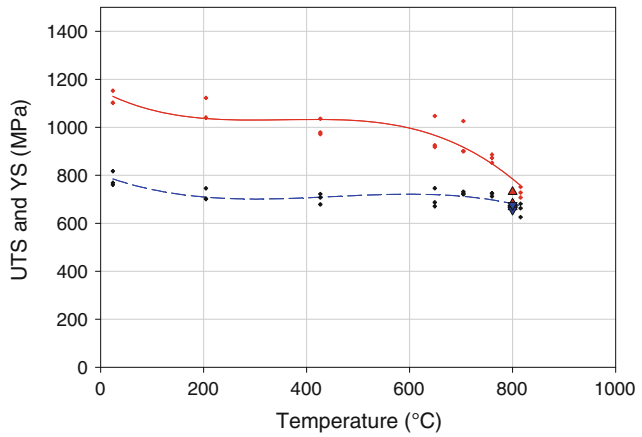

Fig. 9. Comparison of the UTS (solid line) and YS (dashed line) for peak aged wrought N105 from room temperature to 816°C versus the cast and peak aged N105 at 800°C. Triangular symbols represent cast N105.

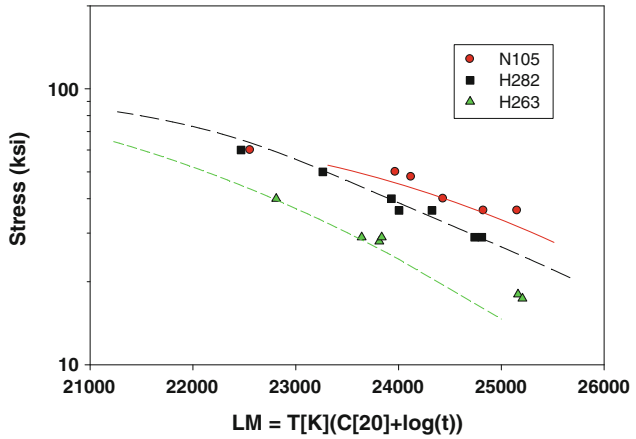

Fig. 10. Comparison of the creep performance of the cast alloys (individual data points) with the average wrought alloy creep performance (lines).

CONCLUSIONS

The phase stability predicted in the region of 760°C to 800°C for the three alloys examined in this study shows that they all form γ' and $M_{23}C_6$ as the major strengthening components within the γ matrix. The η and μ phases were predicted for equilibrium conditions, but they appear to be kinetically limited and have not been observed.

The equilibrium solidification range for all alloys was less than 100°C, while the nonequilibrium (Scheil determined) solidification range was ~200°C.

A computationally optimized homogenization heat treatment was utilized to reduce/eliminate the as-cast microsegregation.

Fluidity studies on alloy 263 and H282 showed that the fluidity of these alloys monotonically increased with increasing superheat. Furthermore, their fluidity compared favorably to several steels. No hot tears were observed on any of the castings.

The creep performance of all three alloys compared favorably to their wrought counterparts, making these alloys good candidates for further evaluation as cast materials for large components such as steam turbine casings.

Table III. Summary of selected tensile properties for N105, alloy 263, and H282 in the wrought and peak aged condition and in the cast, homogenized, and peak aged condition

Test Temperature (°C)	N105		Alloy 263		H282	
	0.2% YS (MPa)	Elongation (%)	0.2% YS (MPa)	Elongation (%)	0.2% YS (MPa)	Elongation (%)
RT	782	27	580	39	721	28
760	721	17	496	21	640	41
800	664	11	355	10	473	23
816	656	11	463	6	572	46

Tensile results at 800°C correspond to the cast alloys, while all others are for wrought form.

REFERENCES

1. R. Viswanathan, et al., *J. Mater. Eng. Perform.* 14, 281–292 (2005).
2. R. Viswanathan, A.F. Armor, and G. Booras, *Power* 4, 42–49 (2004).
3. http://www.netl.doe.gov/technologies/coalpower/advresearch/Ultrasupercritical.html. Accessed 15 Dec 2011.
4. THERMO-CALC, Version S (Stockholm: Royal Institute of Technology, 2008).
5. P.D. Jablonski and C.J. Cowen, *Metall. Mater. Trans.* 40B, 182 (2009).
6. P.D. Jablonski and C.J. Cowen, filed with the U.S. Patent Office (August, 2009).
7. H.F. Taylor, E.A. Rominski, and C.W. Briggs, *Trans AFS* 49, 1 (1941).
8. P.D. Jablonski, *Proceedings of the 2005 International Symposium on Liquid Metal Processing and Casting*, ed. P.D. Lee, A. Mitchell, R.L. Williamson, and A.S. Ballantyne (Materials Park, OH: ASM International, 2005), p. 113.
9. E. Scheil, *Z. Metallkd.* 34, 70–72 (1942).
10. G.H. Gulliver, *J. Inst. Met.* 9, 120–157 (1913).
11. DICTRA, version 25 (Stockholm: Royal Institute of Technology, 2008).
12. G.A. Lillieqvist, Transactions. *Trans. AFS* 58, 261 (1950).